Influence of lattice dynamics on lithium-ion conductivity: A first-principles study

Arun K. Sagotra, Dewei Chu, and Claudio Cazorla
School of Materials Science and Engineering, University of New South Wales Australia, Sydney, New South Wales 2052, Australia

(Received 18 November 2018; revised manuscript received 3 March 2019; published 28 March 2019)

In the context of novel solid electrolytes for solid-state batteries, first-principles calculations are becoming increasingly more popular due to their ability to reproduce and predict accurately the energy, structural, and dynamical properties of fast-ion conductors. To accelerate the discovery of new superionic conductors is convenient to establish meaningful relations between ionic transport and simple materials descriptors. Recently, several experimental studies on lithium fast-ion conductors suggested a correlation between lattice softness and enhanced ionic conductivity due to a concomitant decrease in the activation energy for ion migration E_a. In this article, we employ extensive *ab initio* molecular dynamics simulations based on density functional theory to substantiate the links between ionic transport and lattice dynamics in a number of structurally and chemically distinct lithium superionic conductors. Our first-principles results show no evidence for a direct and general correlation between E_a, or the hopping attempt frequency ν_0, and lattice softness. However, we find that, in agreement with recent observations, the pre-exponential factor of lithium diffusivity D_0, which is proportional to ν_0, follows the Meyer-Neldel rule $\propto \exp(E_a/\langle\omega\rangle)$ where $\langle\omega\rangle$ represents an average phonon frequency. Hence, lattice softness can be identified with enhanced lithium diffusivity, but only within families of superionic materials presenting very similar migration activation energies due to an increase in D_0 (or, equivalently, in ν_0). On the technical side, we show that neglecting temperature effects in the estimation of E_a may lead to huge inaccuracies of $\sim$10%. The limitations of zero-temperature harmonic approaches in describing the vibrational properties of lithium-ion conductors are also illustrated.

DOI: 10.1103/PhysRevMaterials.3.035405

I. INTRODUCTION

Fast-ion, or superionic, conductors (FIC) exhibit large ionic conductivies ($\sim$1 mS cm^{-1}) in the crystal phase [1]. Examples of archetypal FIC are CaF_2, AgI, and $La_{0.5}Li_{0.5}TiO_3$ [2–4]. In addition to their fundamental interests, FIC are of tremendous importance in technological applications such as solid-state batteries [5], solid oxide fuel cells [6], solid-state cooling [7–10], and catalysis and sensors [11,12]. In the context of electrochemical energy storage, lithium FIC are critical for enabling the back-and-forth passage of lithium ions between electrodes in solid-state batteries. Lithium FIC, however, are complex materials in which ionic conductivity depends strongly on their composition, chemical bonding, and atomic structure, and thus far only a reduced number of fast-ion conductors have been identified as suitable electrolytes [5]. Then to accelerate the design novel lithium FIC with enhanced ionic conductivities is desirable to establish meaningful relationships between lithium diffusivity and simple materials descriptors [13,14].

Recent studies explored the correlations between lattice dynamics and ionic transport in lithium-based and other families of FIC [15–20]. In particular, Kraft *et al.* investigated the superionic argyrodites Li_6PS_5X (X = Cl, Br, I) [19] and Muy *et al.* the LISICON series derived from Li_3PO_4 [20] with electrochemical impedance spectroscopy and neutron diffraction techniques. The authors of both studies concluded that lattice softness correlates with low activation energies for ion migration E_a. The intuitive explanation for such an effect is that low-frequency lattice excitations involve large atomic displacements around the equilibrium positions, which may enhance the probability of lithium ions to hop towards adjacent sites [5,20,21].

On a fundamental scale, it would be very interesting to ascertain whether the same interplay between E_a and lattice dynamics could be generalized to other families of lithium FIC presenting markedly different compositions and structural traits (e.g., cubic antiperovskites and hexagonal nitride and oxide compounds—we recall that Li_6PS_5X and Li_3PO_4-based compounds mostly exhibit orthorhombic crystal symmetry). Meanwhile, the intuitive explanation that was proposed to understand the influence of phonons on lithium-ion conductivity might be too simplistic. For instance, lithium ions are lightweight hence the low-frequency lattice excitations in FIC, which are mostly related to the mechanical stiffness of the material, generally will be dominated by heavier atomic species. Intuitively, then it could be argued that wide anion lattice vibrations would reduce the excursions of lithium ions (e.g., by distorting the usual low-dimensional ion conducting channels [22]) and thus obstruct, rather than enhance, their diffusivity. Moreover, large lithium displacements around the equilibrium positions also involve low vibrational frequencies, which suggests a reduction in the corresponding hopping attempt frequency. This last effect would have an opposite impact on the ionic conductivity than an eventual decrease in E_a, and *a priori* it is not clear which of the two mechanisms would be dominant [19]. For an improved design of lithium FIC, a more general and quantitative understanding of how lattice dynamics and ionic transport are related is crucially needed.

First-principles simulations may help at improving our comprehension of FIC via accurate estimation of ion-migration energy barriers, relevant thermodynamic properties, and preferred diffusion paths [23–25]. Nevertheless, due to the intense computational expense associated to first-principles calculations, most quantum studies of FIC generally neglect temperature effects. Unfortunately, this simplification may lead to important bias and errors in the predictions. For instance, zero-temperature calculations of ion-migration energy barriers customarily are performed with the nudged-elastic band (NEB) method [26], in which the initial and final geometries of the vacancy or interstitial ions need to be guessed in the form of high-symmetry metastable states; the limitations of this method for determining the preferred ion-diffusion paths are well documented for some prototype FIC-like metal halogens (e.g., CaF_2 [25,27] and PbF_2 [28,29]), copper chalcogenides (e.g., Cu_2S [30]), and lithium-based oxides (e.g., $LiFePO_4$ [31]).

Likewise, phonon calculations customarily are performed at zero temperature by using harmonic approximations [32–34] and considering perfectly stoichiometric systems (i.e., with full Li occupancy); such simplifications may result in a misrepresentation of real lithium FIC in which sizable ionic conductivities normally appear at high temperatures and in nonstoichiometric compounds (i.e., with partial Li occupancy) [5,20]. Actually, superionic phases in lithium FIC tend to be highly anharmonic and become entropically stabilized at $T \neq 0$ K conditions (that is, imaginary phonon frequencies usually appear in the corresponding zero-temperature phonon spectra), as we show in Fig. 1 (see also Supplemental Fig. 1 [35] and Refs. [2,17,20,36]). It thus seems apparent that considering temperature effects in first-principles simulations of FIC is actually necessary for better understanding them [37].

Ab initio molecular dynamics (AIMD) simulations naturally account for temperature and anharmonic effects in materials, and thus are a powerful tool for analyzing accurately and with reliability ionic diffusion processes in FIC [2,38–41]. Estimation of key quantities like jump rates, hopping attempt frequencies, correlation factors, and T-dependent phonon frequencies, which are not accessible with zero-temperature methods, can be obtained directly from AIMD simulations. The superior performance of AIMD methods certainly comes with a significant increase in computational expense; however, due to the current steady growth in computational power, improved design of algorithms, and the fact that lithium FIC typically can be described with a relatively small number of valence electrons (by using pseudopotential approaches), reliable AIMD simulation of fast-ion materials is currently within reach (see works [2,38–41] and Supplemental Material [35]).

In this article, we present a thorough study on the lattice dynamics and ionic transport properties of several distinct lithium FIC based on density functional theory AIMD simulations. Specifically, we analyze the lithium diffusivity and T-dependent density of vibrational states in the following compounds (space groups are indicated within parentheses): hexagonal Li_3N ($P6_3/mmc$) [42], orthorhombic $LiGaO_2$ ($Pna2_1$) [43], cubic LiF ($Fm\bar{3}m$) [44], hexagonal $LiIO_3$ ($P6_3$) [45], tetragonal Li_3OCl ($P4/mmm$) [46], and tetragonal $Li_{10}GeP_2S_{12}$ ($P4_2/nmc$) [47–49]. Lattice phonons and activation energies for ion migration are calculated at zero-temperature conditions in most cases to quantify the impact of temperature and anharmonic effects on their evaluation [50].

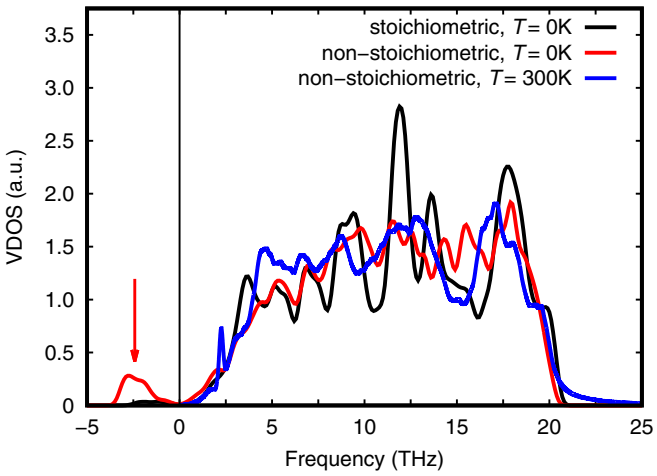

FIG. 1. Vibrational density of states of Li_3N calculated at different compositions and temperatures. (*Black*) Stoichiometric system at zero temperature is vibrationally unstable since it exhibits few imaginary phonon frequencies; results are obtained with the harmonic approximation. (*Red*) Nonstoichiometric system at zero temperature is vibrationally unstable since it exhibits many imaginary phonon frequencies, most of which are associated with Li-dominated lattice eigenmodes (indicated by the red arrow); results are obtained with the harmonic approximation. (*Blue*) Nonstoichiometric system at $T = 300$ K is vibrationally stable due to the lack of imaginary phonon frequencies; results are obtained with AIMD simulations, which fully take into consideration anharmonicity and temperature effects.

Our simulation results demonstrate the lack of a direct and general correlation between E_a, or the hopping attempt frequency of lithium ions ν_0, and $\langle\omega\rangle$, where the latter term represents the average phonon frequency of the crystal (either associated to all the compound atoms or just to Li ions). However, we show that ν_0 follows the Meyer-Neldel rule $\propto \exp(E_a/\langle\omega\rangle)$, in consistent agreement with recent experimental observations [51]. Thus crystal anharmonicity, or equivalently lattice softness, can be identified with enhanced ionic diffusivity but only within families of FIC that present inherently similar migration activation energies. On the technical side, we quantify the systematic errors in E_a and $\langle\omega\rangle$ that result from neglecting temperature effects, which unexpectedly turn out to be quite large (e.g., a typical $\sim$10% underestimation of migration activation energies). Our theoretical work provides an improved understanding of how lattice dynamics influences lithium conductivity in FIC, hence it may be useful for improving the design of energy storage and energy conversion devices.

II. SIMULATION METHODS

A. First-principles calculations

First-principles calculations based on density functional theory (DFT) are performed to analyze the vibrational and ionic transport properties of lithium FIC. We perform these calculations with the VASP code [52] by following the

generalized gradient approximation to the exchange-correlation energy due to Perdew *et al.* [53]. (Possible dispersion interactions in Li_3N [10] are captured with the *D*3 correction scheme developed by Grimme *et al.* [54].) The projector-augmented-wave method is used to represent the ionic cores [55], and the following electronic states are considered as valence: Li 1*s*-2*s*, N 2*s*-2*p*, Ga 4*s*-4*p*, O 2*s*-2*p*, F 2*s*-2*p*, I 5*s*-5*p*, Ge 4*s*-4*p*, P 3*s*-3*p*, S 3*s*-3*p*, and Cl 3*s*-3*p*. Wave functions are represented in a plane-wave basis truncated at 650 eV. By using these parameters and dense **k**-point grids for Brillouin zone integration, the resulting energies are converged to within 1 meV per formula unit. In the geometry relaxations, a tolerance of $0.01\,\text{eV}\cdot\text{Å}^{-1}$ is imposed on the atomic forces.

AIMD simulations based on DFT are performed in the canonical (N, V, T) ensemble (i.e., constant number of particles, volume, and temperature) for all the considered bulk materials. The selected V's correspond to the equilibrium volumes determined at zero temperature, hence we neglected thermal expansion effects; nevertheless, we performed some molecular dynamics tests and found that thermal expansion effects do not affect significantly the estimation of diffusion coefficients and activation energies in the selected Li FIC (that is, below 5%, see Supplemental Material [35]). The concentration of lithium vacancies in the nonstoichiometric systems has been also considered independent of T and equal to ∼2%. The temperature in the AIMD simulations is kept fluctuating around a set-point value by using Nose-Hoover thermostats. Large simulation boxes containing $N_{\text{ion}} \sim 250$ atoms are employed in all the cases, and periodic boundary conditions are applied along the three Cartesian directions. Newton's equations of motion are integrated by using the customary Verlet's algorithm and a timestep length of $\delta t = 10^{-3}$ ps. Γ-point sampling for integration within the first Brillouin zone is employed in all the AIMD simulations. The calculations comprise long simulation times of $t_{\text{total}} \sim 200$ ps.

For each compound, we typically run a total of 8 AIMD simulations at different temperatures and considering both stoichiometric and nonstoichiometric systems; this number of simulations turns out to be sufficient to obtain accurate estimation of the corresponding diffusion coefficients and activation energies (see next section and Supplemental Materials [35]). We focus on the description of the superionic and vibrational properties of lithium FIC, which are estimated by monitoring the positions and velocities of the ions during the AIMD simulations. Tests performed on the numerical bias stemming from the finite size of the simulation cell and duration of the molecular dynamics runs are reported in the Supplemental Materials [35]. In view of the results obtained in those numerical tests, the adopted N_{ion} and t_{total} values can be assumed to provide reasonably well-converged results for the ionic diffusivity and vibrational density of states of lithium FIC. Further details of our AIMD simulations (e.g., exact simulation cell dimensions, duration of the runs, concentration of vacancies, number of AIMD runs, and temperatures) can be found in the Supplemental Table I [35].

Zero-temperature phonon frequency calculations are performed with the small-displacement method, in which the force-constant matrix is calculated in real-space by considering the proportionality between atomic displacements and forces [32,33,56,57]. The quantities with respect to which our phonon calculations are converged include the size of the supercell, the size of the atomic displacements, and the numerical accuracy in the sampling of the Brillouin zone. We find the following settings to provide quasiharmonic free energies converged to within 5 meV per formula unit: $3 \times 3 \times 3$ supercells, typically containing 200–300 ions (the figures indicate the number of replicas of the unit cell along the corresponding lattice vectors), atomic displacements of 0.02 Å, and **q**-point grids of $14 \times 14 \times 14$. The value of the phonon frequencies are obtained with the PHON code developed by Alfè [57]. In using this code we exploit the translational invariance of the system to impose the three acoustic branches to be exactly zero at the center of the Brillouin zone, and apply central differences in the atomic forces.

Ab initio nudged-elastic band (NEB) calculations [26] are performed to estimate the energy barriers for ionic diffusion in the investigated lithium FIC at zero temperature. Our NEB calculations typically are performed in $2 \times 2 \times 2$ or $3 \times 3 \times 3$ supercells containing several tens of atoms. We use **q**-point grids of $8 \times 8 \times 8$ or $6 \times 6 \times 6$ and an energy plane-wave cutoff of 650 eV. Six intermediate images are used to determine the most likely ion-diffusion paths in the absence of temperature. The geometry optimizations are halted when the total forces on the atoms are smaller than $0.01\,\text{eV}\cdot\text{Å}^{-1}$.

B. Estimation of key quantities

The mean square displacement (MSD) is estimated with the formula

$$\text{MSD}(\tau) = \frac{1}{N_{\text{ion}}(N_{\text{step}} - n_\tau)} \times \sum_{i=1}^{N_{\text{ion}}} \sum_{j=1}^{N_{\text{step}}-n_\tau} |\mathbf{r}_i(t_j + \tau) - \mathbf{r}_i(t_j)|^2, \quad (1)$$

where $\mathbf{r}_i(t_j)$ is the position of the migrating ion i at time t_j $(= j \cdot \delta t)$, τ represents a lag time, $n_\tau = \tau/\delta t$, N_{ion} is the total number of mobile ions, and N_{step} the total number of time steps (equivalent to ∼200 ps). The maximum n_τ is chosen equal to $N_{\text{step}}/2$ (equivalent to ∼100 ps), hence we can accumulate enough statistics to reduce significantly the fluctuations in $\text{MSD}(\tau)$ at large τ's (see the size of the error bars in the MSD plots presented in the following sections). The diffusion coefficient then is obtained by using the Einstein relation

$$D = \lim_{\tau\to\infty} \frac{\text{MSD}(\tau)}{6\tau}. \quad (2)$$

In practice, we consider $0 < \tau \leqslant 100$ ps and estimate D by performing linear fits over the averaged $\text{MSD}(\tau)$ values calculated in the interval $50 \leqslant \tau \leqslant 100$ ps.

The T dependence of the diffusion coefficient is assumed to follow the Arrhenius formula

$$D(T) = D_0 \cdot \exp\left[-\frac{E_a}{k_B T}\right], \quad (3)$$

where D_0 is known as the pre-exponential factor, E_a is the activation energy for ionic migration, and k_B the Boltzmann

constant. From a physical point of view, D_0 can be interpreted as a hopping attempt frequency, ν_0, the value of which is obtained via the relationship

$$\nu_0 = \frac{D_0}{a_0^2}, \tag{4}$$

where a_0 represents the equilibrium lattice parameter of the crystal (that is, a characteristic length for the ionic hops). Likewise, the exponential factor in Eq. (3) can be interpreted as an acceptance probability for the proposed ionic jumps. Hence large (small) D_0 and small (large) E_a lead to high (low) ionic conductivities.

To estimate the density of vibrational states in lithium FIC considering anharmonic effects, VDOS, we calculate the Fourier transform of the velocity-velocity autocorrelation function obtained directly from the AIMD simulations as

$$\mathrm{VDOS}(\omega) = \frac{1}{N_{\mathrm{ion}}} \sum_i^{N_{\mathrm{ion}}} \int_0^\infty \langle \mathbf{v}_i(\tau) \cdot \mathbf{v}_i(0) \rangle e^{i\omega\tau} d\tau, \tag{5}$$

where $\mathbf{v}_i(t)$ represents the velocity of the atom labeled as i at time t, and $\langle \cdots \rangle$ denotes the statistical average in the (N, V, T) ensemble. We note that other methods than employed here can be also used to estimate T-dependent VDOS beyond the harmonic approximation [58–60]. Once the density of vibrational states is known, it is straightforward to calculate the corresponding phonon band center or average lattice frequency $\langle \omega \rangle$, defined as

$$\langle \omega \rangle = \frac{\int_0^\infty \mathrm{VDOS}\, \omega\, d\omega}{\int_0^\infty \mathrm{VDOS}\, d\omega}, \tag{6}$$

which also depends on T. Likewise, the contribution of a particular group of ions to the full VDOS can be estimated by considering them alone in the summation appearing in Eq. (5). To determine a characteristic low-energy phonon frequency for lithium FIC, we (somewhat arbitrarily) define the quantity

$$\langle \omega \rangle_{\mathrm{room}} = \frac{\int_0^{\omega_{\mathrm{room}}} \mathrm{VDOS}\, \omega\, d\omega}{\int_0^{\omega_{\mathrm{room}}} \mathrm{VDOS}\, d\omega}, \tag{7}$$

where ω_{room} is $k_B T_{\mathrm{room}}/\hbar = 6.25$ THz.

III. RESULTS

A. Li_3N

This compound presents two common polymorphs known as α and β phases. The α phase (hexagonal, space group $P6/mmm$) has a layered structure composed of alternating planes of hexagonal Li_2N and pure Li^+ ions (see, for instance, Fig. 1 in Ref. [10]). The β phase (hexagonal, space group $P6_3/mmc$) exhibits an additional layer of lithium ions intercalated between consecutive Li_2N planes that is accompanied by a doubling of the unit cell [Fig. 2(a)]. Exceptionally high ionic conductivities of the order of 10^{-4}–10^{-3} S cm^{-1} were measured experimentally in Li_3N at room temperature [42,61,62]. Here we restrict our analysis to β–Li_3N.

Figure 2(a) shows the minimum ion migration activation energy calculated for Li_3N at zero temperature with the NEB method, E_a^0. The local minimum-energy points correspond to lithium vacancy positions since we were not able to generate any metastable interstitial configuration for the stoichiometric system. This outcome suggests that superionicity in Li_3N is vacancy mediated, hence it mostly occurs in nonstoichiometric systems. In good agreement with previous zero-temperature DFT results reported by Li *et al.* [42], we find that the minimum E_a^0 amounts to 0.03 eV and corresponds to lithium diffusion in the region between consecutive Li_2N planes lying along the z direction [Fig. 2(a)]. Thus ionic diffusion seems to be mostly confined to two dimensions, which we denote here as x-y. We note that the migration

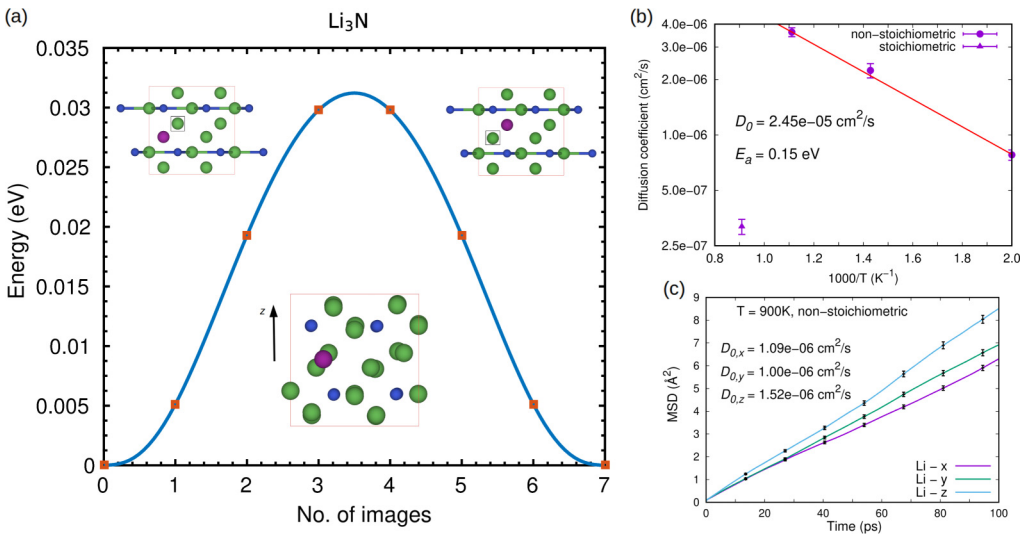

FIG. 2. Activation energy for ion migration calculated for Li_3N at (a) $T = 0$ K and (b) finite temperatures considering lithium vacancies. (c) Ionic diffusivity estimated along the three Cartesian axis in nonstoichiometric Li_3N at $T = 900$ K. Lithium and nitrogen ions are represented with large green and small blue spheres, respectively. Lithium vacancy positions are indicated with black squares and mobile ions with purple spheres. Numerical uncertainties are represented by error bars.

activation energy determined in experiments, E_a^{expt}, is 0.45 eV [42], which is significantly larger than E_a^0.

Figures 2(b) and 2(c) show the results of our AIMD simulations performed at finite temperatures. In accordance with the zero-temperature results just explained, lithium conductivity appears to be vacancy mediated since the diffusion coefficients calculated in the stoichiometric system are too small at high temperatures [namely, $D < 10^{-6}\,\text{cm}^2\text{s}^{-1}$ at $T > 1000\,\text{K}$, Fig. 2(b)]. However, the lithium diffusion mechanisms and activation energy that are deduced from the $T \neq 0\,\text{K}$ simulations differ appreciably from those obtained with zero-temperature methods. In particular, the lithium ions are found to diffuse almost equally along all three Cartesian directions [Fig. 2(c)], and the estimated activation energy is much larger, $E_a = 0.15 \pm 0.02\,\text{eV}$ [Fig. 2(b)]. Although the agreement between the estimated and experimentally measured activation energies has been improved, there is still a considerable difference with respect to E_a^{expt}. A likely explanation for such a discrepancy may be the neglecting of defects other than vacancies in the AIMD simulations (e.g., cracks, dislocations, and interfaces), which in some cases are known to deplete ionic diffusivity significantly [63,64]. Another possibility is that the concentration of extrinsic vacancies in our AIMD simulations probably is too large (that is, ∼2%), which may lead to an overestimation of lithium conductivity. Meanwhile, we estimate a pre-exponential factor of $D_0 = 2.5 \pm 1.0 \cdot 10^{-5}\,\text{cm}^2\text{s}^{-1}$ and a hopping attempt frequency, ν_0, of ∼0.01 THz.

Figure 3(a) shows the density of vibrational states, VDOS, estimated for nonstoichiometric Li_3N at several temperatures with AIMD methods. The system is vibrationally stable in all the cases since no imaginary phonon frequencies appear in the corresponding phonon spectra. This outcome is contrary to the results obtained with the harmonic approximation at zero temperature, which indicate that nonstoichiometric Li_3N is vibrationally unstable (see Fig. 1); we note that the imaginary eigenfrequency phonon modes appearing in that zero-temperature harmonic VDOS are mostly dominated by Li ions (see Supplemental Fig. 2 [35]). As the temperature is increased, the peaks of the VDOS become smoothed and the resulting phonon band center $\langle\omega\rangle$ increases steadily (due to the fact that higher-frequency vibrational modes are thermally activated). The accompanying increase in $\langle\omega\rangle$, however, is very mild. For instance, the phonon band center amounts to 11.66 THz at room temperature and to 11.74 THz at $T = 700\,\text{K}$. The average phonon frequency that is estimated by applying a cutoff of $k_B T_{\text{room}}/\hbar$ to the VDOS, $\langle\omega\rangle_{\text{room}}$ [Eq. (7)], provides a characteristic frequency for the low-energy phonons of the material, which are mostly related to its mechanical stiffness. We find that the T-induced variation of such a frequency is also very moderate; for example, at $T = 700\,\text{K}$ $\langle\omega\rangle_{\text{room}}$ is ∼1% larger than the value estimated at ambient conditions, which is 4.7 THz.

We note that at $T = 700\,\text{K}$ nonstoichiometric Li_3N is superionic and presents a large diffusion coefficient of $2.2 \cdot 10^{-6}\,\text{cm}^2\text{s}^{-1}$ whereas at room temperature remains in the normal state ($D \sim 0$). Hence in Li_3N does not seem possible to correlate the large T-induced variations in ionic conductivity with the accompanying changes in VDOS, which are minute (i.e., of the order of ∼0.1 THz). Figures 3(b) and 3(c) show the partial VDOS corresponding to lithium and nitrogen ions, respectively. The partial phonon band center of the nitrogen ions is lower than $\langle\omega\rangle_{\text{Li}}$ by ∼3%, as it could have been foreseen due to their larger atomic mass (recall the $m_\alpha^{-1/2}$ factors entering the expression of the dynamical force constant matrix [32–34]). Interestingly, low anion vibration phonon excitations have been recently linked to a reduction in FIC stability against electrochemical oxidation [20].

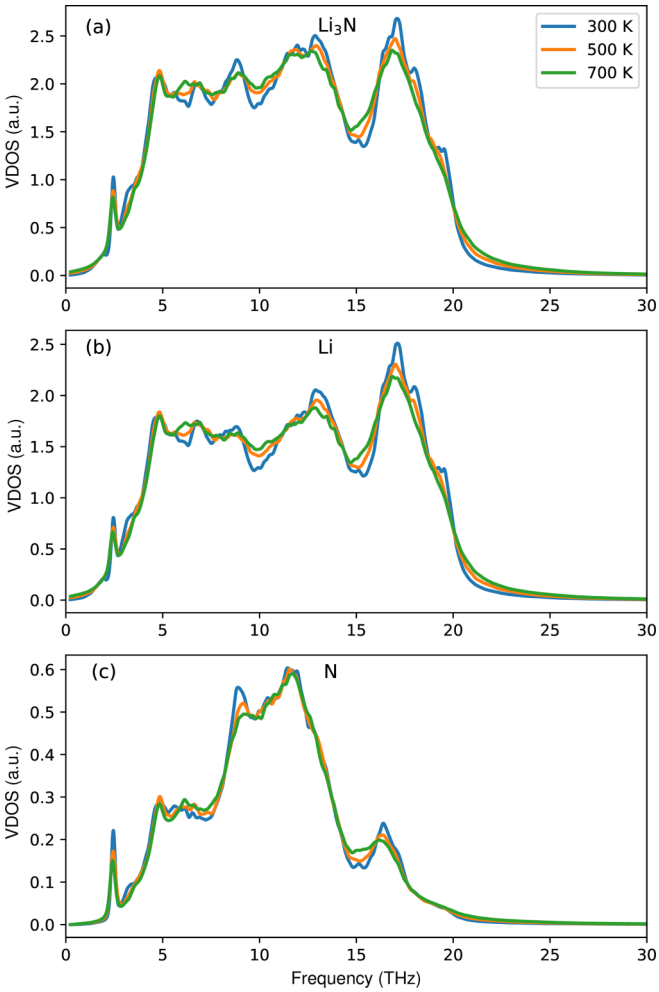

FIG. 3. Density of vibrational states calculated for Li_3N at different temperatures considering (a) all the atoms, (b) only Li ions, and (c) only N ions. Results are obtained from the Fourier transform of the velocity-velocity autocorrelation function calculated during long AIMD simulations.

B. $LiGaO_2$

At ambient conditions this compound stabilizes in a orthorhombic structure with space group $Pna2_1$. The lithium and gallium ions are located at the center of oxygen tetrahedrons, forming a two-dimensional stacking of alternating LiO_4 and GaO_4 arrays. Recently, a combined experimental and theoretical study proved the superionic nature of $LiGaO_2$ at temperatures $T \geqslant 800\,\text{K}$ [43].

Figures 4(a) and 4(b) show the activation energy for Li interstitial and vacancy migration calculated at zero temperature with the NEB method. In this case, we were able

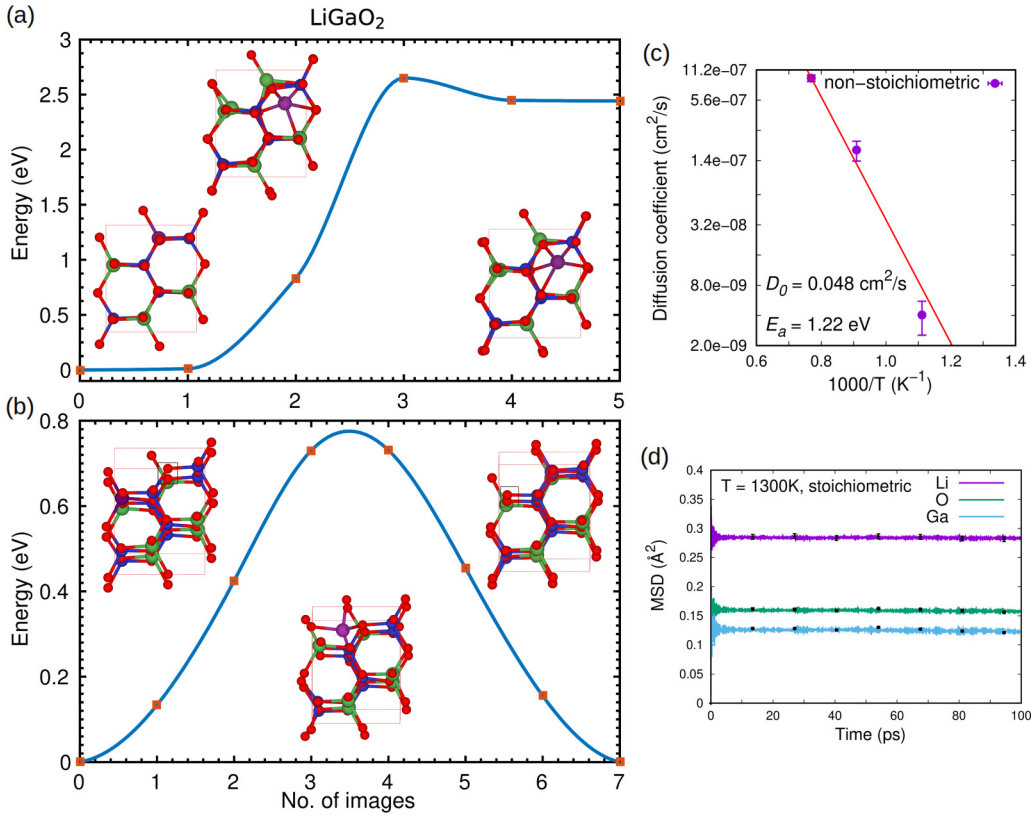

FIG. 4. Activation energy for ion migration calculated for $LiGaO_2$ at zero-temperature considering (a) interstial and (b) vacancy positions. (c) Lithium diffusivity of nonstoichiometric $LiGaO_2$ calculated at finite temperatures. (d) Mean square displacement of stoichiometric $LiGaO_2$ calculated at very high temperatures. Lithium, gallium, and oxygen ions are represented with large green, small blue, and small red spheres, respectively. Lithium vacancy positions are indicated with black squares and mobile ions with purple spheres. Numerical uncertainties are represented by error bars.

to generate a metastable interstitial configuration for the stoichiometric system, as shown in Fig. 4(a); however, the accompanying zero-temperature interstitial formation energy and activation migration energy appear to be too large, namely, 2.4 and 2.6 eV respectively. Meanwhile, the estimated zero-temperature activation energy for vacancy migration is considerably lower, $E_a^0 = 0.78$ eV [Fig. 4(b)]. These results suggest that fast-ion conductivity in $LiGaO_2$ is also vacancy mediated, which is in agreement with previous NEB DFT calculations reported by Islam *et al.* [43]. We note, however, that the experimentally measured activation energy for Li migration is $E_a^{\text{expt}} = 1.25$ eV [43], which is significantly larger than the predicted E_a^0. A possible explanation for the significant discrepancy between the measured and calculated zero-temperature activation energies could be the neglection of temperature effects in NEB simulations, as it has been suggested by the authors of Ref. [43].

Our AIMD results shown in Fig. 4(c) confirm that after considering temperature effects the agreement between the estimated and measured activation energies improves drastically. In particular, we calculate a large E_a of 1.2 ± 0.1 eV, which practically coincides with the corresponding experimental value. Likewise, the computed pre-exponential factor is $5.0 \pm 1.5 \cdot 10^{-2}\,\text{cm}^2\text{s}^{-1}$, which leads to a very large ν_0 of $\sim$10 THz. In agreement with the zero-temperature results explained above, lithium conductivity in $LiGaO_2$ appears to be vacancy mediated since even at high temperatures of $T > 1000$ K the stoichiometric system remains in the normal state [Fig. 4(d)].

We have estimated the VDOS of nonstoichiometric $LiGaO_2$ at several temperatures with AIMD methods (Supplemental Fig. 3 [35]). The system is vibrationally stable in all the cases since no imaginary phonon frequencies appear in the corresponding phonon spectra. The effect of temperature on the calculated VDOS is very small and similar to that described previously for Li_3N. For instance, the average phonon frequency $\langle\omega\rangle$ amounts to 11.74 THz at $T = 900$ K and to 11.83 THz at 1300 K. Thus, again the large diffusion coefficient changes induced by temperature ($\Delta D/D \sim 10^2$ for $\Delta T = 400$ K) do not appear to be reflected on the corresponding VDOS ($\Delta\langle\omega\rangle/\langle\omega\rangle \sim 10^{-2}$ for the same ΔT). An analagous increase of about 1% is found for $\langle\omega\rangle_{\text{room}}$, which at $T = 900$ K amounts to 4.4 THz. Regarding the partial VDOS, we find that $\langle\omega\rangle_{\text{Ga}} = 0.6\langle\omega\rangle_{\text{Li}}$ and $\langle\omega\rangle_{\text{O}} = 1.2\langle\omega\rangle_{\text{Li}}$, thus, on average, the Ga ions vibrate at lower frequencies than the lithium ions while the oxygen atoms at higher. Despite the larger mass of the oxygen atoms as compared to lithium, $\langle\omega\rangle_{\text{O}}$ is the highest because oxygen atoms participate in all covalent bonds in the crystal and therefore appear represented across the whole VDOS (Supplemental Fig. 3 [35]). Consequently, the presence of oxygens in Li FIC will tend to increase the phonon band center of the anion sublattice; this effect,

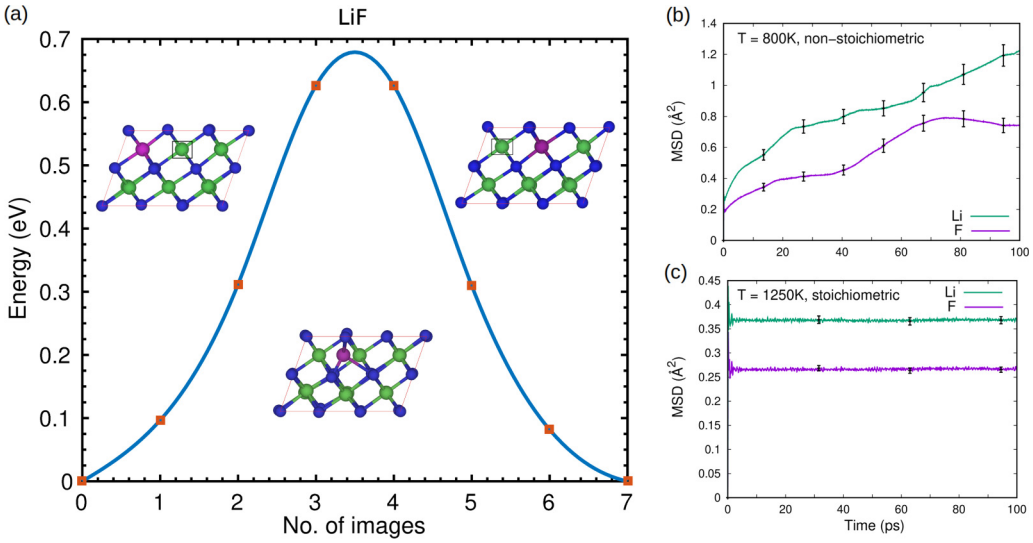

FIG. 5. (a) Activation energy for ion migration calculated for LiF at zero-temperature considering vacancy positions. (b) Mean square displacement of nonstoichiometric LiF calculated at high temperatures. (c) Mean square displacement of stoichiometric LiF calculated at very high temperatures. Lithium and fluorine ions are represented with large green and small blue spheres, respectively. Lithium vacancy positions are indicated with black squares and mobile ions with purple spheres. Numerical uncertainties are represented by error bars.

however, is likely to be reduced significantly in the presence of other electronegative species presenting larger atomic masses (e.g., sulfur) [20].

C. LiF

The crystal structure of bulk LiF at ambient conditions is rocksalt (cubic, space group $Fm\bar{3}m$). The presence of LiF has been revealed in the interface between the solid electrolyte and electrodes in Li-ion batteries [65], and the accompanying effects on energy storage performance were investigated recently by several authors with theory [44,66,67].

By performing NEB calculations, we estimate a zero-temperature energy barrier for lithium vacancy diffusion of $E_a^0 = 0.68$ eV [Fig. 5(a)], which is in very good agreement with previous DFT calculations [44,66,67]. We note that in this case we could neither find a metastable interstitial configuration, hence ionic conductivity in LiF in principle also appears to be vacancy mediated. The E_a^0 calculated for LiF is comparable to that determined previously for $LiGaO_2$, suggesting that lithium diffusivity in both materials should be similar. However, our AIMD simulations show that this is not the case. In particular, at temperatures above 700 K nonstoichiometric LiF becomes vibrationally unstable, as shown by the fact that both the lithium and fluorine ions are drifting [Fig. 5(b)]. Consequently, we have not been able to determine any E_a or D_0 for bulk LiF. This outcome highlights the importance of crystal structure and composition on lithium conductivity: two materials with similar E_a^0 but different geometries and chemical bonds may not be comparable in terms of ionic diffusivity. Meanwhile, our AIMD simulations show that lithium conduction in stoichiometric LiF is negligible even at high temperatures [that is, $D \sim 0$ at $T > 1000$ K, Fig. 5(c)], in agreement with the zero-temperature NEB calculations.

The T-dependent VDOS of nonstoichiometric LiF calculated with AIMD simulations are reported in Supplemental Fig. 4 [35]. The corresponding average phonon frequency amounts to 9.19 THz at $T = 400$ K and to 9.45 THz at 600 K. Hence, despite the fact that LiF is a much worse lithium conductor than, for instance, Li_3N, its phonon band center is significantly lower (e.g., $\langle\omega\rangle = 11.70$ THz at $T = 500$ K for nonstoichiometric Li_3N). Such a comparison suggests the lack of a direct correlation between lattice dynamics and lithium diffusivity in the investigated systems; we will comment on this point with more detail later. Regarding the partial VDOS, we find that $\langle\omega\rangle_F = 0.7\langle\omega\rangle_{Li}$ owing to the larger mass of the fluorine ions and the ionic nature of the material. Thus, the low-frequency lattice excitations in LiF ($\omega < 5$ THz) clearly are dominated by the F ions, not the lithium.

D. $LiIO_3$

At ambient conditions this compound stabilizes in a hexagonal phase (space group $P6_3$) in which each iodine atom is surrounded by three oxygen atoms, forming a three-dimensional net of tightly bound pyramidal IO_3^- groups [Fig. 6(a)]. $LiIO_3$ exhibits a complex polymorphism and may undergo reconstructive phase transitions by effect of pressure and temperature [68,69]. More than four decades ago, Aliev *et al.* experimentally investigated the mobility of lithium ions in this compound [45]. They concluded that ionic diffusion occurred within quasi-one-dimensional channels oriented along the hexagonal c-axis, with a corresponding activation energy of $E_a^{expt} = 0.26$ eV [45]. To the best of our knowledge, the lithium diffusion mechanisms in $LiIO_3$ have not been studied previously with first-principles methods.

By using NEB calculations, we estimate a zero-temperature activation energy of $E_a^0 = 0.09$ eV for lithium vacancies diffusing along the hexagonal c direction [Fig. 6(a)]. This result is significantly smaller than the corresponding experimental value. Nevertheless, our AIMD simulations render $E_a = 0.36 \pm 0.07$ eV [Fig. 6(b)], which is larger than E_a^0 and provides a better agreement with the observations. Likewise, the calculated pre-exponential factor is

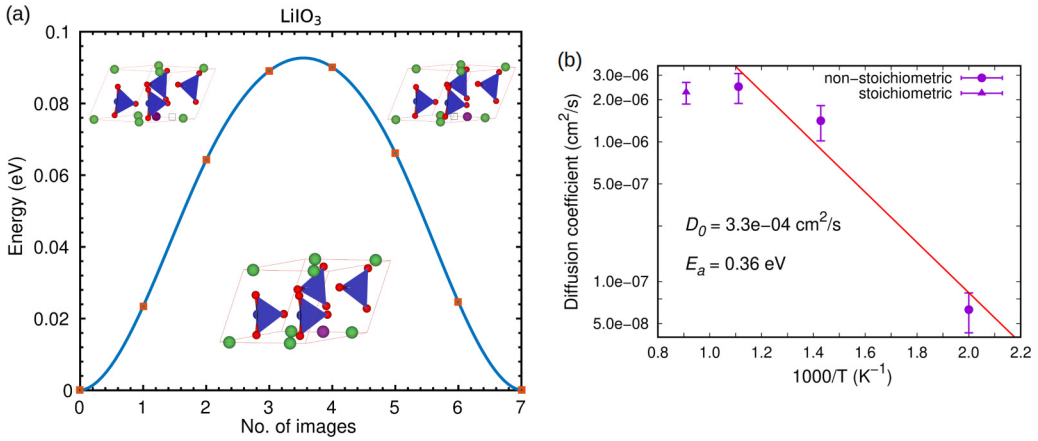

FIG. 6. (a) Activation energy for ion migration calculated for $LiIO_3$ at zero-temperature considering vacancy positions. (b) Lithium diffusivity of nonstoichiometric and stoichiometric $LiIO_3$ calculated at finite temperatures. Lithium, iodine, and oxygen ions are represented with large green, small blue, and small red spheres, respectively. Lithium vacancy positions are indicated with black squares and mobile ions with purple spheres. Numerical uncertainties are represented by error bars.

$3.5 \pm 1.5 \cdot 10^{-4}\,\mathrm{cm^2 s^{-1}}$ and the resulting hopping attempt frequency $\sim$0.1 THz. Large diffusion coefficients are estimated also for stoichiometric $LiIO_3$, although at temperatures well above ambient conditions [Fig. 6(b)].

The VDOS calculated for nonstoichiometric $LiIO_3$ at $T \neq 0$ K conditions are reported in Supplemental Fig. 5 [35]. The total phonon band center amounts to 9.82 THz at room temperature and increases to 9.92 THz at $T = 700$ K. Once again, the huge changes induced by temperature on the diffusion coefficient ($\Delta D/D \sim 10^3$ for $\Delta T = 400$ K) are not reflected on the corresponding VDOS ($\Delta\langle\omega\rangle/\langle\omega\rangle \sim 10^{-2}$ for the same ΔT). We also note that although the E_a estimated for $LiIO_3$ is about two times larger than estimated for Li_3N, the average phonon frequency in the former compound is noticeably smaller (namely, 9.82 and 11.66 THz, respectively, at T_{room}). In analogy to $LiGaO_2$, we find that the oxygen ions render the largest $\langle\omega\rangle$ whereas the heaviest cations the smallest ($\langle\omega\rangle_{\mathrm{I}} = 0.4\langle\omega\rangle_{\mathrm{Li}}$); in this case, the low-frequency lattice excitations ($\omega < 5$ THz) are clearly dominated by the oxygen and iodine ions (Supplemental Fig. 5 [35]).

E. Li_3OCl

This compound presents an antiperovskite structure similar to that of archetypal ABO_3 perovskite oxides [46,70,71]. Specifically, the Li, O, and Cl ions are placed at octahedral vertices, octahedral centers, and cube vertices, respectively. (We note that in our zero-temperature geometry relaxations the Li_3OCl unit cell presents a c/a ratio of 0.97; hence, our symmetry labeling as tetragonal $P4/mmm$ rather than cubic $Pm\bar{3}m$.) The main mechanism for ion migration in Li_3OCl was proposed to be vacancy diffusion accompanied by anion disorder [24,46,72].

Our zero-temperature NEB calculations render $E_a^0 = 0.37$ eV for lithium vacancy diffusion [Fig. 7(a)], which is in good agreement with previous first-principles results [24,72] and the experimental value $E_a^{\mathrm{expt}} = 0.26$ eV [46]. Our AIMD simulations, however, provide a much larger value of the lithium migration enery barrier, namely, $E_a = 0.90 \pm 0.05$ eV [Fig. 7(b)]. The corresponding pre-exponential factor is also very large, $D_0 = 1.4 \pm 0.5 \cdot 10^{-2}\,\mathrm{cm^2 s^{-1}}$, which leads to a high hopping attempt frequency of $\sim$10 THz (very similar to the one estimated for $LiGaO_2$). A possible cause for the large discrepancy between E_a^{expt} and E_a may be the presence of a higher concentration of anion disorder and lithium vacancies in the experimental samples (in our AIMD simulations we considered only vacancies at a small concentration of $\sim$2%). Meanwhile, our AIMD simulations confirm that lithium diffusivity in stoichiometric Li_3OCl is negligible [24,72], even at high temperatures of $T > 1000$ K [Fig. 7(c)].

The VDOS calculated for nonstoichiometric Li_3OCl considering anharmonic and temperature effects are reported in Supplemental Fig. 6 [35]. The total phonon band center amounts to 8.90 THz at $T = 1000$ K and increases to 9.08 THz at $T = 1250$ K. Like in the previous cases, the huge changes induced by temperature on the diffusion coefficient ($\Delta D/D \sim 10^1$ for $\Delta T = 250$ K) do not translate into significant VDOS variations ($\Delta\langle\omega\rangle/\langle\omega\rangle \sim 10^{-2}$ for the same ΔT). We also note that although the E_a calculated for Li_3ClO is about three times larger than the estimated for $LiIO_3$, the total average phonon frequency of both compounds are quite similar (8.9 and 9.9 THz, respectively, at $T \sim 1000$ K). In analogy to previous cases, we find that the oxygen ions render the largest $\langle\omega\rangle$ whereas the heaviest cations the smallest ($\langle\omega\rangle_{\mathrm{Cl}} = 0.5\langle\omega\rangle_{\mathrm{Li}}$). On the other hand, the low-frequency lattice excitations ($\omega < 5$ THz) are dominated by the lithium and chlorine ions (Supplemental Fig. 6 [35]).

F. $Li_{10}GeS_2P_{12}$

This compound was recently introduced by Kamaya *et al.* [47] and has attracted significant interest because at room temperature its Li ionic conductivity is comparable, or even superior, to that of liquid electrolytes. $Li_{10}GeS_2P_{12}$ is the most representative of thio-LISICON materials, which are chemically analogous to LISICON but where oxygen ions are replaced by sulfur. The crystal structure of $Li_{10}GeS_2P_{12}$ possesses tetragonal symmetry (space group $P4_2/nmc$) and consists of LiS_6 octahedra linked by $(Ge/P)S_4$ tetrahedra

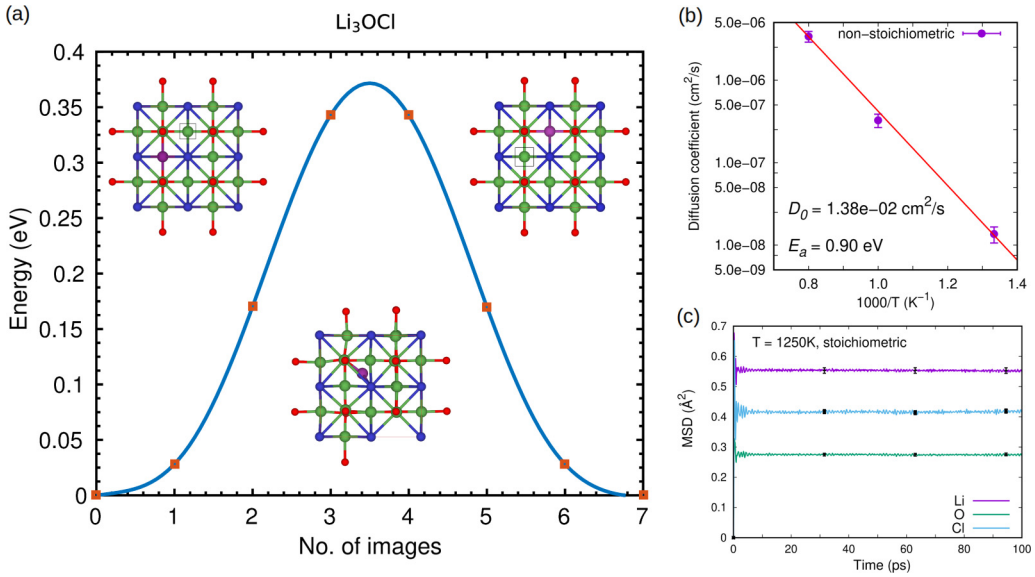

FIG. 7. (a) Activation energy for ion migration calculated for Li_3OCl at zero-temperature considering vacancy positions. (b) Lithium diffusivity of nonstoichiometric Li_3OCl calculated at finite temperatures. (c) Mean square displacement of stoichiometric Li_3OCl calculated at very high temperatures. Lithium, chlorine, and oxygen ions are represented with large green, small blue, and small red spheres, respectively. Lithium vacancy positions are indicated with black squares and mobile ions with purple spheres. Numerical uncertainties are represented by error bars.

{Fig. 8(a)]. In this particular case, we perform AIMD simulations just considering perfectly stoichiometric systems.

The VDOS calculated for stoichiometric $Li_{10}GeP_2S_{12}$ at $T \neq 0$ K conditions are reported in Supplemental Fig. 7 [35]. This system is particularly anharmonic (or, equivalently, vibrationally soft) as shown by its large concentration of phonon modes at low frequencies, which leads to the estimation of very small $\langle\omega\rangle$ values. For instance, the total phonon band center amounts to 7.46 THz at $T = 650$ K and just increases slightly to 7.53 THz at 1150 K. Once again, the large changes induced by temperature on the diffusion coefficient ($\Delta D/D \sim 10^1$ for $\Delta T = 500$ K) are not reproduced by the corresponding VDOS ($\Delta\langle\omega\rangle/\langle\omega\rangle \sim 10^{-2}$ for the same ΔT). The E_a that we estimate for this compound amounts to 0.17 ± 0.02 eV [Fig. 8(b)], which is in quite good agreement with the experimental value $E_a^{\text{expt}} = 0.25$ eV [47], and other theoretical results reported in previous AIMD studies [48,49]. We note that the zero-temperature activation energy estimated for $Li_{10}GeP_2S_{12}$ by other authors is significantly smaller than E_a^{expt}, namely, $E_a^0 = 0.09$ eV [49]. Meanwhile, the pre-exponential factor that we calculate is $3.0 \pm 0.7 \cdot 10^{-4}$ cm^{2}s^{-1} and the resulting hopping attempt frequency ~0.1 THz.

It is worth noting that although the E_a's estimated for $Li_{10}GeP_2S_{12}$ and Li_3N are very similar (Table I), the corresponding average phonon frequencies are noticeably different (namely, 7.46 and 11.74 THz at similar temperatures). Moreover, in analogy to previous cases (e.g., Li_3OCl and $LiIO_3$) we find that the low-frequency lattice excitations ($\omega < 5$ THz) are not dominated by the lithium ions (Supplemental Fig. 7 [35]). For instance, we estimate that almost independently of T $\langle\omega\rangle_{\text{Ge–P–S}} = 0.95\langle\omega\rangle_{\text{Li}}$, which indicates a

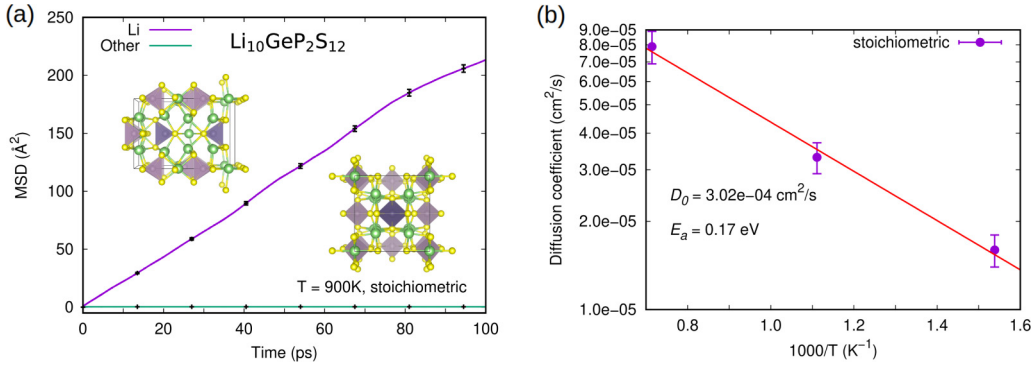

FIG. 8. (a) Mean squared displacement of stoichiometric $Li_{10}GeP_2S_{12}$ calculated at $T = 900$ K; ball-stick representations of the crystal structure from different perspectives are also presented (Li and S atoms are represented with large green and small yellow spheres, respectively, and Ge and P atoms are enclosed within the tetrahedra). (b) Lithium diffusivity of stoichiometric $Li_{10}GeP_2S_{12}$ calculated at finite temperatures. Numerical uncertainties are represented by error bars.

TABLE I. Summary of the activation energies for ion migration calculated at zero and finite temperatures for the different lithium FIC considered in this study. Experimental values for E_a are reported for comparison purposes. The accompanying pre-exponential factors of lithium diffusivity, D_0, and corresponding hopping attempt frequencies ν_0 are enclosed along with the energy scale of the lattice phonon excitations calculated at room temperature $\langle\omega\rangle_{\text{room}}$ (estimated by using a frequency cutoff of $k_B T_{\text{room}}/\hbar$ on the total density of vibrational states).

Material	E_a^0 (eV)	E_a (eV)	E_a^{expt} (eV)	D_0 (cm^2/s)	ν_0 (s^{-1})	$\langle\omega\rangle_{\text{room}}$ (s^{-1})
Li_3N	0.03	0.15 ± 0.02	0.45 [42]	$2.5 \pm 1.0 \cdot 10^{-5}$	$\sim 10^{10}$	$4.7 \cdot 10^{12}$
$LiGaO_2$	0.78	1.2 ± 0.1	1.25 [43]	$5.0 \pm 1.5 \cdot 10^{-2}$	$\sim 10^{13}$	$4.4 \cdot 10^{12}$
LiF	0.68	–	–	–	–	$5.0 \cdot 10^{12}$
$LiIO_3$	0.09	0.36 ± 0.07	0.26 [45]	$3.5 \pm 1.5 \cdot 10^{-4}$	$\sim 10^{11}$	$4.2 \cdot 10^{12}$
Li_3OCl	0.37	0.90 ± 0.05	0.26 [46]	$1.4 \pm 0.5 \cdot 10^{-2}$	$\sim 10^{13}$	$4.4 \cdot 10^{12}$
$Li_{10}GeP_2S_{12}$	0.09 [49]	0.17 ± 0.02	0.25 [47]	$3.0 \pm 0.7 \cdot 10^{-4}$	$\sim 10^{11}$	$3.8 \cdot 10^{12}$

balanced presence of Li, Ge, P, and S ions in most vibrational modes.

IV. DISCUSSION

Table I encloses a summary of the main results obtained for the six lithium FIC analyzed in this study. Next we comment on (i) the importance of considering temperature effects on the estimation of migration activation energies and phonon frequencies in lithium FIC, and (ii) the correlations between superionic descriptors and lattice dynamics that can be deduced from our AIMD simulations.

A. Temperature effects on E_a and $\langle\omega\rangle$

The differences between columns E_a^0 and E_a in Table I provide a quantitative estimate of how much temperature effects may influence the calculation of migration energy barriers in lithium FIC. In the present study, temperature effects account for as much as 35–80% of the final migration activation energies (straightforwardly estimated as $|E_a - E_a^0|/E_a$). Meanwhile, we showed that, except for Li_3OCl, the inclusion of temperature effects always brings into better agreement the calculated and measured migration energy barriers (Table I). Therefore, we argue that AIMD simulations are strongly recommended when pursuing accurate estimation of migration energy barriers (and of lithium diffusion mechanisms as well), in spite of the much larger computational load involved as compared to zero-temperature methods.

LiF, for example, illustrates very well the convenience of performing finite-temperature simulations. This material appears to be a very poor lithium-ion conductor [44,66,67], however, a relatively moderate migration energy barrier of $E_a^0 = 0.68\,\text{eV}$ is calculated with $T = 0\,\text{K}$ methods. Such a value turns out to be quite similar to the E_a^0 obtained for other promising ionic conductors (e.g., 0.78 eV for $LiGaO_2$ [43]), hence one could easily arrive at the wrong conclusion that LiF is a potentially good superionic material.

Interestingly, we appreciate that the calculated E_a's are systematically higher than the corresponding values estimated at zero temperature. This observation could be interpreted such that thermally activated anion lattice vibrations actually tend to deplete lithium transport (since in zero-temperature E_a^0 calculations the anion sublattice remains static). However, other possible temperature effects associated with the diffusion of mobile ions (e.g., entropic stabilization of diverse transition paths) and the complex interactions between cations and anions, could also come into play. In the next subsection, we will comment in detail on the correlations between lithium conductivity (E_a and D_0) and $\langle\omega\rangle$ that can be drawn from our AIMD results.

With regard to the estimation of average phonon frequencies, we note that the harmonic approximation may be not adequate for describing lithium FIC due to the high degree of anharmonicity that superionic phases normally present [17,36,37]. We explicitly demonstrated this in Fig. 1, where the zero-temperature vibrational spectrum of non-stoichiometric Li_3N is shown to contain a considerable number of imaginary phonon frequencies, in contrast to the VDOS obtained at realistic $T \neq 0\,\text{K}$ conditions; we checked that $LiIO_3$ and Li_3OCl behave in a very similar manner (Supplemental Fig. 8 [35]). In fact, the inherent limitations of the harmonic approximation may lead to misinterpretations of the vibrational stability of lithium FIC, and to biased estimation of average phonon frequencies. For instance, we find that $\langle\omega\rangle$ is about 2% larger for Li_3N at zero temperature than at T_{room}, and that such discrepancies propagate to the partial VDOS. It goes without saying that the presence of negative phonon frequencies in zero-temperature VDOS automatically invalidates any estimation of $\langle\omega\rangle$ due to the violation of the fundamental assumptions employed in harmonic approaches [32,33]. For an improved interpretation of experiments, it is very important to avoid the explained computational artifacts by using finite-temperature simulation methods, since partial VDOS normally cannot be resolved directly from the measurements and first-principles calculations are employed instead for that end [20,73].

B. Lattice dynamics versus migration activation energy and pre-exponential factor

In Fig. 9(a), we plot the E_a and $\langle\omega\rangle$ results obtained for the superionic compounds considered in this study. A direct correlation between migration activation energies and average phonon frequencies cannot be established. (One arrives at the same conclusion when representing $\langle\omega\rangle$ as a function of either E_a^{expt} or E_a^0, see Supplemental Fig. 9 [35]). For instance, Li_3N and $LiGaO_2$ present the smallest and largest

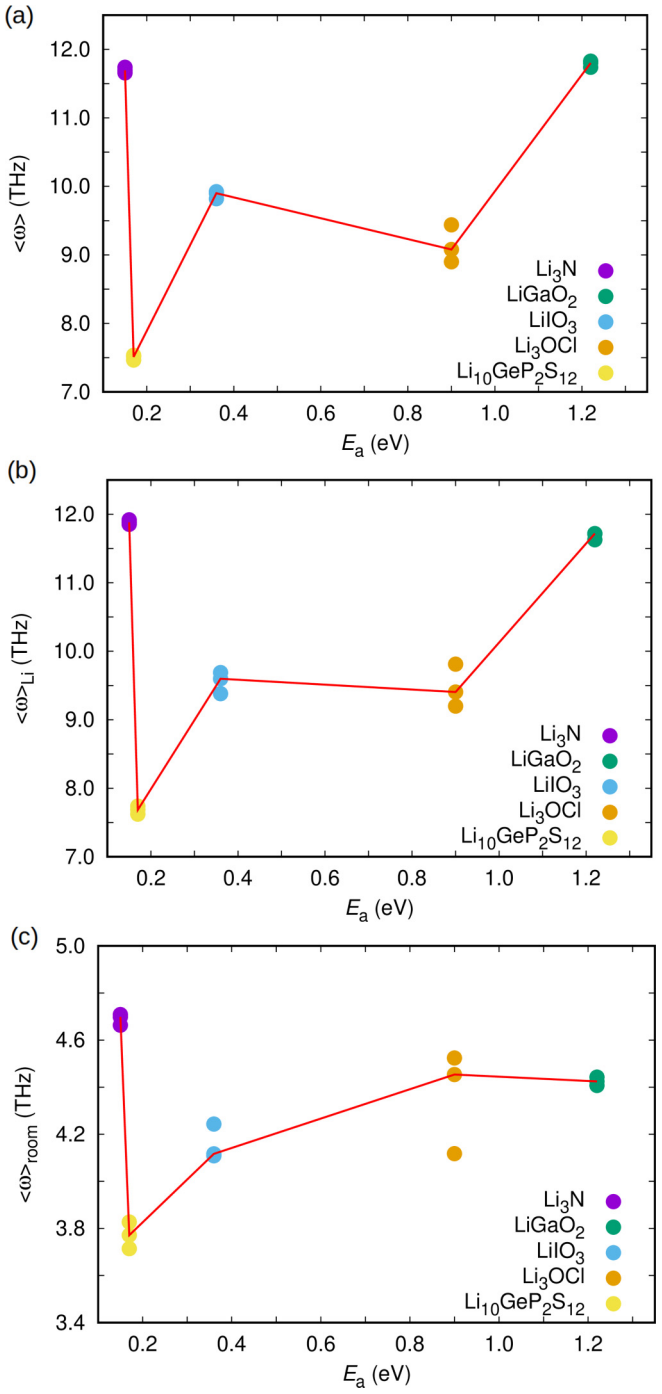

FIG. 9. Phonon band center versus the activation energy barrier for ion migration calculated in lithium FIC considering (a) all the atoms in the crystal, (b) only the Li ions, and (c) all the atoms in the crystal and a frequency cutoff of $k_B T_{\text{room}}/\hbar$. Solid lines are guides to the eye.

E_a, respectively, with a large difference of ∼1 eV, however, the corresponding $\langle\omega\rangle$ turn out to be very similar; moreover, Li_3N and $Li_{10}GeP_2S_{10}$ present the largest and smallest $\langle\omega\rangle$, respectively, with a large difference of ∼4 THz, however, the corresponding E_a turn out to be very similar. Likewise, one concludes the lack of any robust connection between either $\langle\omega\rangle_{\text{Li}}$ or $\langle\omega\rangle_{\text{room}}$ and E_a [Figs. 9(b), 9(c) and Table I]. Hence the correspondence between lattice softness and low activation energies recently suggested for superionic argyrodites and Li_3PO_4-based LISICON [19,20] is not reproduced by our AIMD simulations and consequently should not be generalised to other lithium FIC.

In previous sections we showed that when lithium FIC are analyzed individually, the large enhacements in ionic conductivity induced by temperature are not accompanied by noticeable changes in VDOS. In particular, we obtained large diffusivity variations of $\Delta D/D \sim 10^1 - 10^3$ and only minute vibrational changes of $\Delta\langle\omega\rangle/\langle\omega\rangle \sim 10^{-2}$. Hence, the generalised insensitivity of $\langle\omega\rangle$ to large D fluctuations already suggests the lack of a direct correlation between E_a and $\langle\omega\rangle$ across different families of lithium FIC.

Supplemental Fig. 10 [35] encloses the D_0 and $\langle\omega\rangle$ results obtained for the superionic compounds investigated in this study. Once again, we cannot determine any rigorous correspondence between the two represented quantities. We note that the calculated hopping attempt frequencies fluctuate between 0.01 and 10 THz whereas all the estimated $\langle\omega\rangle$ consistently amount to ∼10 THz (Table I). Therefore, lithium hops and lattice vibrations seem to operate at very different time scales which hints at the cause of their disconnection.

C. Hopping attempt frequency versus E_a

The similarity between the E_a–$\langle\omega\rangle$ and D_0–$\langle\omega\rangle$ trends shown in Fig. 9(a) and Supplemental Fig. 10 [35] appears to suggest some sort of correlation between E_a and D_0. In fact, the conventional hopping theory developed by Rice and Roth provides the well-known, and usually reported, relationship $D_0 \propto \sqrt{E_a}$ [74]. However, we should note that conventional hopping theory was originally developed to understand ionic transport in AgI and other similar type-I FIC [1,8,9], in which the superionic transition is accompanied by a first-order structural transformation in the static sublattice (in contrast to lithium FIC, typically referred to as type-II, in which the superionic transition normally is of second-order type and only affects the mobile ions [1,8]). Therefore, it is possible that conventional hopping theory might not describe Li FIC correctly. Interestingly, a recent experimental study by Muy *et al.* provided solid evidence showing that the interplay between D_0 on E_a may actually be more complex than typically thought [51].

Figure 10(a) reports the D_0 and E_a results that we have obtained in this study. In our case, the two represented quantities appear to be correlated since larger migration activation energies systematically are accompanied by larger pre-exponential factors. However, we note that the usually reported relationship $D_0 \propto \sqrt{E_a}$ [74] clearly does not pertain here (we recall that the y-axes in Figs. 10(a) and 10(b) are in logarithmic scale). Rather, the dependence of D_0 on E_a appears to be exponential like. Recently, Muy *et al.* showed that the diffusion pre-exponential factors of a large number of LISICON compounds follow the Meyer-Neldel rule $D_0 \propto \exp(E_a/\langle\omega\rangle)$ [51]. In fact, when we represent the computed diffusion pre-exponential factors as a function of the quantity $E_a/\langle\omega\rangle$ we find a good agreement with the Meyer-Neldel rule within our numerical uncertainties [see linear fit in Fig. 10(b)]. Compounds $Li_{10}GeP_2S_{12}$ and Li_3OCl do not lie exactly on

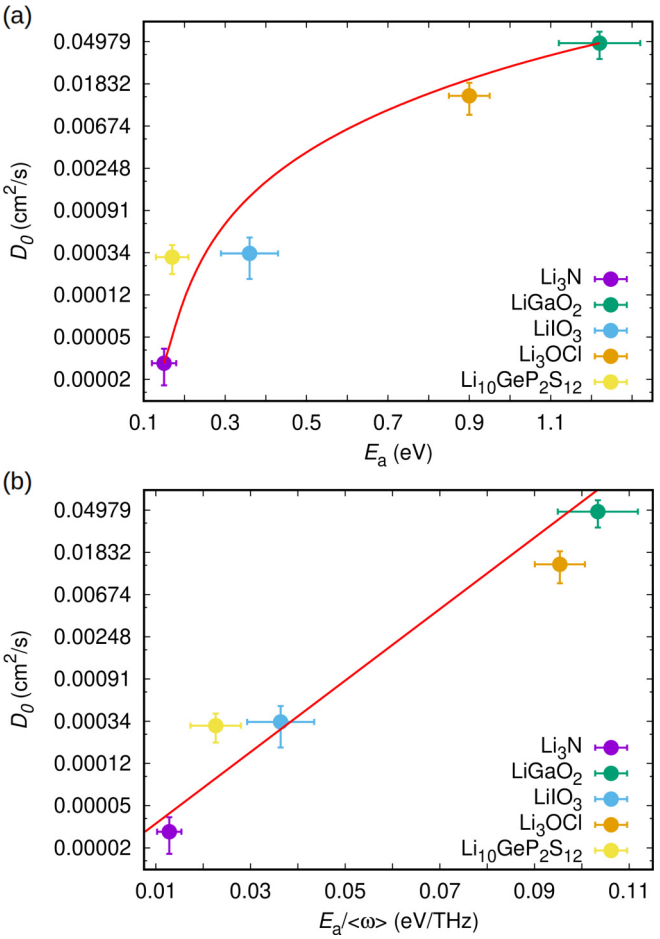

FIG. 10. Lithium diffusivity pre-exponential factor (in logarithmic scale) versus the (a) activation energy barrier for ion migration (the solid line is a guide to the eye), and (b) ratio of the activation energy barrier for ion migration and phonon band center (the solid line corresponds to a linear fit). Numerical uncertainties are represented by error bars.

the extrapolated exponential curve but remain very close to it. Our theoretical findings, therefore, seem to confirm Muy *et al.*'s conclusions reported in work [51] and show that Rice and Roth's hopping theory in general is not adequate for describing lithium FIC.

The results and discussions presented thus far let us to conclude the following: lattice softness can be identified with enhanced lithium diffusivity but only within families of superionic materials presenting very similar migration activation energies due to larger D_0 or, equivalently, larger ν_0 (as given by the Meyer-Neldel rule). We should note that according to our zero-temperature and AIMD simulations lithium partial occupancy in FIC can be identified with enhanced anharmonicity or, equivalently, smaller $\langle\omega\rangle$. For instance, the average phonon frequency calculated for nonstoichiometric Li_3N at finite temperatures is about 1% lower than the estimated for the analogous stoichiometric system. Hence lattice softness may indeed be a key factor for better understanding the ionic transport differences between stoichiometric and non-stoichiometric lithium FIC which are structurally and chemically very similar [51].

V. CONCLUSION

We performed a comprehensive first-principles study of several (purposely chosen) different lithium FIC at finite temperatures. Based on our AIMD results, it was not possible to establish any direct correlation between either E_a or D_0 and $\langle\omega\rangle$, in disagreement with recent experimental findings reported for superionic argyrodites and Li_3PO_4-based LISICON. Reassuringly, we showed that the spectra of lattice vibrations in lithium FIC generally are very insensitive to temperature changes, in contrast to what was observed for ionic transport, and that the lithium hopping attempt frequencies and average phonon frequencies have associated very different timescales. Nevertheless, the three quantities E_a, D_0, and $\langle\omega\rangle$ appear to be related by the Meyer-Neldel rule, in accordance with recent measurements; hence, on a general scale it is possible to identify lattice softness with enhanced ionic conductivity but only within families of FIC presenting very similar migration activation energies, owing to an increase in the hopping attempt frequency. On the technical side, we demonstrated that zero-temperature methods present some inherent limitations for describing Li-based FIC. In particular, migration activation energies can be seriously underestimated due to the neglect of temperature effects, and harmonic approaches may be ill-defined due to the prominent role of anharmonicity in superionicity. We hope that our theoretical findings will help at discriminating physically meaningful relationships between ionic transport and simple materials descriptors in lithium FIC. Also, we expect to promote a wider use of finite-temperature approaches in first-principles modeling of fast-ion conductors.

ACKNOWLEDGMENTS

This research was supported under the Australian Research Council's Future Fellowship funding scheme (No. FT140100135). Computational resources and technical assistance were provided by the Australian Government and the Government of Western Australia through the National Computational Infrastructure (NCI) and Magnus under the National Computational Merit Allocation Scheme and The Pawsey Supercomputing Centre.

[1] S. Hull, Rep. Prog. Phys. **67**, 1233 (2004).
[2] C. Cazorla and D. Errandonea, Phys. Rev. Lett. **113**, 235902 (2014).
[3] D. A. Keen, S. Hull, W. Hayes, and N. J. G. Gardner, Phys. Rev. Lett. **77**, 4914 (1996).
[4] Y. Inaguma, C. Liquan, M. Itoh, T. Nakamura, T. Uchida, H. Ikuta, and M. Wakihara, Solid State Commun. **86**, 689 (1993).
[5] J. C. Bachman, S. Muy, A. Grimaud, H.-H. Chang, N. Pour, S. F. Lux, O. Paschos, F. Maglia, S. Lupart, P. Lamp, L. Giordano, and Y. Saho-Horn, Chem. Rev. **116**, 140 (2016).

[6] R. M. Ormerod, Chem. Soc. Rev. **32**, 17 (2003).
[7] C. Cazorla and D. Errandonea, Nano Lett. **16**, 3124 (2016).
[8] A. K. Sagotra, D. Errandonea, and C. Cazorla, Nat. Commun. **8**, 963 (2017).
[9] A. Aznar, P. Lloveras, M. Romanini, M. Barrio, J. Ll. Tamarit, C. Cazorla, D. Errandonea, N. D. Mathur, A. Planes, X. Moya, and L. Manosa, Nat. Commun. **8**, 1851 (2017).
[10] A. K. Sagotra, D. Chu, and C. Cazorla, Nat. Commun. **9**, 3337 (2018).
[11] T. Montini, M. Melchionna, M. Monai, and P. Fornasiero, Chem. Rev. **116**, 5987 (2016).
[12] J. B. Goodenough, Solid State Ionics **94**, 17 (1997).
[13] Y. Wang, W. D. Richards, S. P. Ong, L. J. Miara, J. C. Kim, Y. Mo, and G. Ceder, Nat. Mater. **14**, 1026 (2015).
[14] R. Xiao, H. Li, and L. Chen, J. Materiomics **1**, 325 (2015).
[15] P. Goel, M. K. Gupta, R. Mittal, S. Rols, S. J. Patwe, S. N. Achary, A. K. Tyagi, and S. L. Chaplot, J. Mater. Chem. A **2**, 14729 (2014).
[16] T. Krauskopf, C. Pompe, M. A. Kraft, and W. G. Zeier, Chem. Mater. **29**, 8859 (2017).
[17] C. Cazorla and D. Errandonea, Phys. Rev. B **98**, 186101 (2018).
[18] H. Fang and P. Jena, Proc. Natl. Acad. Sci. **114**, 11046 (2017).
[19] M. A. Kraft, S. P. Culver, M. Calderon, F. Bocher, T. Krauskopf, A. Senyshyn, C. Dietrich, A. Zevalkink, J. Janek, and W. G. Zeier, J. Am. Chem. Soc. **139**, 10909 (2017).
[20] S. Muy, J. C. Bachman, L. Giordano, H.-H. Chang, D. L. Abernahy, D. Bansal, O. Delaire, S. Hori, R. Kanno, F. Maglia, S. Lupart, P. Lamp, and Y. Shao-Horn, Energy Environ. Sci. **11**, 850 (2018).
[21] K. Wakamura, Phys. Rev. B **56**, 11593 (1997).
[22] X. He, Y. Zhu, and Y. Mo, Nat. Commun. **8**, 15893 (2017).
[23] Y. Mo, S. P. Ong, and G. Ceder, Chem. Mater. **24**, 15 (2012).
[24] Y. Zhang, Y. Zhao, and C. Chen, Phys. Rev. B **87**, 134303 (2013).
[25] C. Cazorla, A. K. Sagotra, M. King, and D. Errandonea, J. Phys. Chem. C **122**, 1267 (2018).
[26] G. Henkelman, B. P. Uberuaga, and H. Jonsson, J. Chem. Phys. **113**, 9901 (2000).
[27] A. K. Sagotra and C. Cazorla, ACS Appl. Mater. Interf. **9**, 38773 (2017).
[28] J. P. Goff, W. Hayes, S. Hull, and M. T. Hutchings, J. Phys.: Condens. Matter. **3**, 3677 (1991).
[29] M. J. Castiglione and P. A. Madden, J. Phys.: Condens. Matter. **13**, 9963 (2001).
[30] L.-W. Wang, Phys. Rev. Lett. **108**, 085703 (2012).
[31] J. Yang and J. S. Tse, J. Phys. Chem. A **115**, 13045 (2011).
[32] C. Cazorla and J. Boronat, Rev. Mod. Phys. **89**, 035003 (2017).
[33] C. Cazorla and J. Íñiguez, Phys. Rev. B **88**, 214430 (2013).
[34] C. Cazorla, O. Dieguez, and J. Íñiguez, Sci. Adv. **3**, e1700288 (2017).
[35] See Supplemental Material at http://link.aps.org/supplemental/10.1103/PhysRevMaterials.3.035405 for (1) additional details on the vibrational properties of the analysed systems, (2) the representation of $\langle\omega\rangle$ as a function of E_a^{expt} and E_a^0, (3) the representation of D_0 as a function of $\langle\omega\rangle$, (4) additional technical details on our calculations, and (5) the results of a series of numerical tests performed for the calculation of relevant quantities.
[36] M.-H. Chen, A. Emly, and A. Van der Ven, Phys. Rev. B **91**, 214306 (2015).
[37] J. Klarbring and S. I. Simak, Phys. Rev. Lett. **121**, 225702 (2018).
[38] N. J. J. Klerk, E. van der Maas, and M. Wagemaker, ACS Appl. Energy Mater. **1**, 3230 (2018).
[39] B. Singh, M. K. Gupta, R. Mittal, and S. L. Chaplot, J. Mater. Chem. A **6**, 5052 (2018).
[40] W. D. Richards, T. Tsujimura, L. J. Miara, Y. Wang, J. C. Kim, S. P. Ong, I. Uechi, N. Suzuki, and G. Ceder, Nat. Commun. **7**, 11009 (2016).
[41] L. Kahle, A. Marcolongo, and N. Marzari, Phys. Rev. Mater. **2**, 065405 (2018).
[42] W. Li, G. Wu, C. M. Araujo, R. H. Scheicher, A. Blomqvist, R. Ahuja, Z. Xiong, Y. Feng, and P. Chen, Energy Environ. Sci. **3**, 1524 (2010).
[43] M. M. Islam, J. Uhlendorf, E. Witt, H. Schmidt, P. Heitjans, and T. Bredow, J. Phys. Chem. C **121**, 27788 (2017).
[44] H. Yildirum, A. Kinaci, M. K. Y. Chan, and J. P. Greeley, ACS Appl. Mater. Interfaces **7**, 18985 (2015).
[45] A. E. Aliev, A. Sh. Akramov, L. N. Fershtat, and P. K. Khabibullaev, Phys. Status Solidi A **108**, 189 (1988).
[46] Y. Zhao and L. L. Daemen, J. Am. Chem. Soc. **134**, 15042 (2012).
[47] N. Kamaya *et al.*, Nat. Mater. **10**, 682 (2011).
[48] X. He, Y. Zhu, A. Epstein, and Y. Mo, npj Comput. Mater. **4**, 18 (2018).
[49] K. Oh *et al.*, Chem. Mater. **30**, 4995 (2018).
[50] D. Gambino, D. G. Sangiovanni, B. Alling, and I. A. Abrikosov, Phys. Rev. B **96**, 104306 (2017).
[51] S. Muy, J. C. Bachman, H.-H. Chang, L. Giordano, F. Maglia, S. Lupart, P. Lamp, W. G. Zeier, and Y. Shao-Horn, Chem. Mater. **30**, 5573 (2018).
[52] G. Kresse and J. Furthmüller, Phys. Rev. B **54**, 11169 (1996).
[53] J. P. Perdew, K. Burke, and M. Ernzerhof, Phys. Rev. Lett. **77**, 3865 (1996).
[54] S. Grimme, J. Antony, S. Ehrlich, and S. Krieg, J. Chem. Phys. **132**, 154104 (2010).
[55] P. E. Blöchl, Phys. Rev. B **50**, 17953 (1994).
[56] G. Kresse, J. Furthmüller, and J. Hafner, Europhys. Lett. **32**, 729 (1995).
[57] D. Alfè, Comp. Phys. Commun. **180**, 2622 (2009).
[58] P. Souvatzis, O. Eriksson, M. I. Katsnelson, and S. P. Rudin, Phys. Rev. Lett. **100**, 095901 (2008).
[59] O. Hellman, I. A. Abrikosov, and S. I. Simak, Phys. Rev. B **84**, 180301(R) (2011).
[60] I. Errea, M. Calandra, and F. Mauri, Phys. Rev. Lett. **111**, 177002 (2013).
[61] U. V. Alpen, A. Rabenau, and G. H. Talat, Appl. Phys. Lett. **30**, 621 (1977).
[62] G. A. Nazri, C. Julien, and H. S. Mavi, Sol. Stat. Ionics **70**, 137 (1994).
[63] L. Sun, D. Marrocchelli, and B. Yildiz, Nat. Commun. **6**, 6294 (2015).
[64] K. K. Adepalli, J. Yang, J. Maier, H. L. Tuller, and B. Yildiz, Adv. Funct. Mater. **27**, 1700243 (2017).
[65] M. Y. Nie, D. Chalasani, D. P. Abraham, Y. J. Chen, A. Bose, and B. L. Lucht, J. Phys. Chem. C **117**, 1257 (2013).
[66] J. Pan, Y.-T. Cheng, and Y. Qi, Phys. Rev. B **91**, 134116 (2015).

[67] F. A. Soto, A. Marzouk, F. El-Mellouhi, and P. B. Balbuena, Chem. Mater. **30**, 3315 (2018).
[68] J. K. Liang, G. H. Rao, and Y. M. Zhang, Phys. Rev. B **39**, 459 (1989).
[69] W. W. Zhang, Q. L. Cui, Y. W. Pan, S. S. Dong, J. Liu, and G. T. Zou, J. Phys.: Condens. Matter **14**, 10579 (2002).
[70] C. Cazorla and M. Stengel, Phys. Rev. B **92**, 214108 (2015).
[71] C. Cazorla and M. Stengel, Phys. Rev. B **90**, 020101(R) (2014).
[72] Z. Lu, C. Chen, Z. M. Baiyee, X. Chen, C. Niu, and F. Ciucci, Phys. Chem. Chem. Phys. **17**, 32547 (2015).
[73] T. Krauskopf, S. Muy, S. P. Culver, S. Ohno, O. Delaire, Y. Shao-Horn, and W. G. Zeier, J. Am. Chem. Soc. **140**, 14464 (2018).
[74] M. J. Rice and W. L. Roth, J. Solid State Chem. **4**, 294 (1972).